

# Calculation of JVX Proprotor Performance and Comparisons with Hover and High-Speed Test Data

C. W. Acree, Jr.  
 Aeromechanics Branch  
 NASA Ames Research Center  
 Moffett Field, California  
 Cecil.W.Acree@NASA.gov

## Abstract

A 0.658-scale V-22 rotor (the JVX proprotor) was tested at the NASA Ames Research Center in both hover and airplane-mode (high-speed axial flow) flight conditions, up to an advance ratio of 0.562 (231 knots). Both hover and airplane-mode data were used to develop improved aerodynamic models of the JVX proprotor. A multiple-trailer free-wake model was developed for JVX hover analyses. The new model gave improved predictions of hover performance while also giving good predictions of airplane-mode performance. Predictions with simpler aerodynamic models are also included, along with discussions of stall-delay models.

## Notation

DNW	Duits-Nederlandse Windtunnel	$C_T$	rotor thrust coefficient, $T / (\rho A V_{tip}^2)$
LCTR	Large Civil Tiltrotor	$FM$	rotor hover figure of merit, $(T \sqrt{T / 2 \rho A}) / P$
NFAC	National Full-Scale Aerodynamics Complex	$N$	number of blades
OARF	Outdoor Aerodynamic Rotor Facility	$P$	rotor power
PTR	Propeller Test Rig	$P_i$	rotor induced power
TRAM	Tilt Rotor Aeroacoustics Model	$P_o$	rotor profile power
$A$	rotor disk area	$R$	rotor radius
$K_L$	stall-delay factor (Corrigan model)	$T$	rotor thrust
$K_{sdD}$	stall-delay factor for drag (Selig model)	$V$	flight speed
$K_{sdL}$	stall-delay factor for lift (Selig model)	$V_{tip}$	rotor tip speed
$c$	blade chord	$\alpha$	angle of attack
$c_d$	airfoil section drag coefficient	$\alpha_z$	zero-lift angle of attack
$c_{dL}$	linear approximation of drag coefficient	$\eta$	propulsive efficiency, $T V / P$
$c_{dtable}$	drag coefficient from airfoil table	$\Gamma$	blade section circulation
$c_{dz}$	drag coefficient at zero lift	$\kappa$	induced power ratio, $C_{Pi} / C_{Piideal}$
$c_l$	airfoil section lift coefficient	$\kappa_\lambda$	factor on induced velocity
$c_{lL}$	linear extension of lift coefficient	$\mu$	advance ratio, $V / V_{tip}$
$c_{ltable}$	lift coefficient from airfoil table	$r$	local blade radius
$C_P$	rotor power coefficient, $P / (\rho A V_{tip}^3)$	$\sigma$	rotor solidity, $Nc / \pi R$
$C_{Pi}$	induced power coefficient, $P_i / (\rho A V_{tip}^3)$		
$C_{Piideal}$	ideal power coefficient, $C_T^{3/2} / \sqrt{2}$		
$C_{P_o}$	profile power coefficient, $P_o / (\rho A V_{tip}^3)$		

## Introduction

The research reported here was initiated as part of efforts to exploit and extend the results of the NASA Heavy Lift Rotorcraft Systems Investigation (Ref. 1). That effort was directed towards the short-haul civil market, with ambitious efficiency, noise and cost requirements deliberately chosen to stimulate advanced VTOL technology development. The Large Civil Tiltrotor (LCTR) was selected as having the best potential of several configurations to meet NASA technology goals.

---

*Presented at the AHS Specialist's Conference on Aeromechanics, San Francisco, CA, January 23-25, 2008. This material is declared a work of the U. S. Government and is not subject to copyright protection.*

With the LCTR selected as the preferred design, research turned towards increasingly sophisticated proprotor designs. This motivated a re-examination of the analytical tools used to predict rotor performance and the test data used to validate the methodology. The intent was to improve both the accuracy and efficiency of rotor performance predictions, or to at least quantify the tradeoffs between computational speed and numerical accuracy. The emphasis was on proprotors, with higher twist and lower aspect ratio than conventional helicopter rotors.

Whether improved in accuracy or simplified for efficiency, the analytical methods required validation against test data. Exploration of NASA archives uncovered large-scale, airplane-mode JVX proprotor test data that had never been published or thoroughly examined. The JVX rotor was an experimental precursor to the V-22 rotor. Sometimes referred to as a “2/3 scale V-22,” it in fact differed from the V-22 in several respects. It is described in detail below. Complete JVX hover test data were published in Ref. 2, and very limited airplane-mode data from a 1988 test were published in Ref. 3. A much more extensive set of airplane-mode wind-tunnel data acquired in 1991 are published herein for the first time. Both the hover and airplane-mode JVX data are compared with predictions of several levels of sophistication. Limited comparisons with 1/4-scale V-22 data (the TRAM model) are also included.

The proprotor performance code used here is CAMRAD II (Ref. 4). CAMRAD II is a comprehensive rotorcraft analysis code, with a free wake model, a multi-element structural beam model, and a choice of stall delay models. It is much more computationally efficient than any equivalent CFD/CSD code. The latest version (Release 4.6) has an improved free-wake model, specifically a revised distortion integration algorithm for improved accuracy.

For this report, five different levels of aerodynamic modeling were evaluated: uniform inflow, differential momentum (the CAMRAD II implementation of combined blade-element/momentum theory), prescribed wake (based on the Kocurek and Tangler model), rolled-up free wake, and multiple-trailer free wake. In addition, two different, three-dimensional stall-delay models were evaluated. The CAMRAD II wake models have been thoroughly documented elsewhere, notably Ref. 5, and will be briefly discussed in the context of the test data. The stall-delay models, however, merit a more thorough discussion to clarify their differences, which is the purpose of the section entitled “CAMRAD II stall-delay models.”

## The JVX and TRAM Test Rotors

The JVX rotor was tested in two different aerodynamic configurations, so care must be taken when comparing it to the production V-22 rotor and other scaled V-22 rotors, such as TRAM (described later in this section). The following description includes information from Refs. 2 and 3. See also Ref. 6 for JVX airfoil data.

The JVX rotor was 25 feet in diameter, which is 0.658 scale referred to the original V-22 design. However, the production V-22 rotor was slightly enlarged for manufacturing reasons, so the JVX test rotor was more accurately 0.656-scale referred to the present V-22. The JVX rotor used an XV-15 hub with fixed, 2.5-deg precone, whereas the V-22 hub has a coning flexure with slightly different at-rest precone. An XV-15 spinner was used for JVX, instead of the much shorter V-22 spinner. JVX hover testing was done with the original taper, twist and airfoil distribution, with linear taper and an XN-28 airfoil at the root. JVX airplane-mode testing was done with a thicker root section to model the V-22 production blade, which must accommodate a folding hinge. The JVX rotor was always tested when mounted to the Propeller Test Rig (PTR), which has a fairing over the rotor balance just behind the hub (Figs. 1 and 2). The trailing edges at the blade roots were slightly clipped to clear the rotor balance fairing.



Fig. 1. The JVX rotor mounted on the PTR for hover tests at the OARF.



Fig. 2. The JVX rotor mounted on the PTR for airplane-mode tests in the NFAC.

The JVX rotor has spawned several progeny, each with slightly different characteristics. JVX hover performance was better than expected because of 3-D rotational stall-delay effects, which were not well understood at the time, and wing download was underestimated. The full-scale V-22 was subsequently built with slightly lower solidity than JVX and with a blade-fold hinge and fairing. The BA 609 rotor is similar to JVX, but slightly larger in diameter and with a different root airfoil section (Ref. 7). It also has lower solidity than JVX. It is, therefore, identical to neither JVX nor V-22. There are also several small-scale aircraft, such as the Eagle Eye, that use aerodynamically similar rotors. None is an exact scaled version of JVX, and their differences, although sometimes small, must be kept in mind when comparing performance data.

The Tilt Rotor Aeroacoustics Model (TRAM) is a 1/4-scale V-22, designed for acoustics and blade loads measurements (Ref. 8). It has been tested as both a full-span model with two rotors and as an isolated rotor. Figure 3 shows the TRAM isolated-rotor configuration, as

installed in the Duits-Nederlandse Windtunnel (DNW) for airplane-mode tests.

The JVX and TRAM rotor characteristics are summarized in Table 1. The test conditions relevant to this report are summarized in Table 2. Additional details are given in Ref. 9, from which Tables 1 and 2 are adapted.



Fig. 3. TRAM airplane-mode configuration in the DNW.

Table 1. JVX and TRAM rotor characteristics

	JVX	TRAM
scale	0.658-scale V-22	0.25-scale V-22
rotor radius (in)	150	57
solidity (thrust weighted)	0.1138	0.105
tip chord (in)	15.79	5.5
taper (tip/root chord)	0.65	0.62

Table 2. JVX and TRAM summary test conditions

	JVX OARF	JVX 40x80	TRAM hover	TRAM axial
tip Mach no.	0.676	0.575, 0.625	0.628	0.593
tip speed (ft/sec)	754	640, 695	701	662
airspeed (knots)	0	100-231	0	127-147

## JVX and TRAM Rotor Tests

JVX hover tests were performed on the Outdoor Aerodynamic Rotor Facility (OARF), at NASA Ames Research Center, in 1984 (Ref. 2). High-speed (airplane mode) and wing download and interference tests were conducted in the 40- by 80-ft test section of the National Full-Scale Aerodynamics Complex (NFAC) at NASA Ames, divided into three test phases. Phase I tests were conducted in 1988 (Ref. 3). Only very limited airplane-mode data were collected and published, because of control-system problems and difficulties obtaining good tare corrections for the spinner. (The spinner is on the metric side of the rotor balance.) The Phase II entry was in 1991. The Phase II airplane-mode data were never publicly released. Phase III was intended to complete the airplane-mode data set, but the rotor was destroyed in an accident very early in the test.

The airplane-mode data presented here are all from the Phase II data. Although the maximum speed attained was below the desired goal of 300 knots, the data are adequate to validate analyses used for design optimization.

The JVX hover tests were all performed on the OARF (Fig. 1), which was free from recirculation effects and most wall effects (excepting, of course, the ground, as can be seen in the photograph). The test data shown here were all taken near dawn, at very low wind conditions. Although some tests were done with a scaled V-22 wing installed to measure download, all data shown here were taken without the wing and were selected for minimum wind (less than 1 knot).

Some JVX airplane-mode tests were conducted with a wing or with the PTR yawed with respect to the flow, but all data shown here were taken without the wing and at zero yaw angle. Standard test procedure was to set the rotor rpm and tunnel airspeed, then vary collective so as to vary thrust and power at a fixed advance ratio. The data presented here represent five different advance ratios. The criteria for data selection were no wing or yaw, and enough data points at each advance ratio for meaningful comparisons with predictions.

TRAM was tested as an isolated rotor in the DNW in 1988 (Ref. 10). The data presented here are a subset of those in Ref. 10. During the DNW tests, TRAM was operated at 89% design rotor speed in hover, which is reflected in all analyses performed for the present research.

Several hover tests of V-22 scale models are compared to the actual V-22 in Ref. 11, but only the JVX and TRAM DNW test data are for an isolated rotor. While the TRAM rotor has a hub more representative of the V-22, its blade

root is not an exact match to the V-22. Moreover, the isolated-rotor version of TRAM has greater flow blockage than the PTR. The nacelle is 1/4-scale V-22, but not the support mechanism, as can be seen in Fig. 3. Therefore, there is no exactly equivalent data set against which to compare JVX data.

For this report, the JVX rotor data are emphasized over TRAM because of the larger scale, the wider variety of airplane-mode data, and the inherently greater accuracy of the PTR for performance measurements. Because the larger purpose of the present research is to develop improved analytical techniques, quality of the data is considered more important than an exact match to the actual V-22.

## Stall-Delay Models

Proprotors are known to generate much more lift than would be predicted from two-dimensional airfoil section data alone. The rotating blade experiences centrifugal pumping of the airflow, which accelerates the boundary layer and greatly delays stall. The effect is strongest at the root. CAMRAD II does not directly calculate this effect, but provides two different means of correcting 2-D airfoil data to compensate for 3-D stall delay. The dependence upon radius must be specified by the user. Although this complicates the input, it provides for maximum flexibility.

The two stall-delay models are derived from Refs. 12 and 13. Examples of adjustments to 2-D properties for the familiar NACA 0012 airfoil are given in Fig. 4; examples of radial distributions are given in Fig. 5. The section corrections and radial distributions were derived together for each model. Both models include empirical adjustments, but give equally good fits to the JVX data.

The Corrigan model (Ref. 12) shifts the peak lift and stall recovery region upwards along a line defined by the lift curve slope at zero  $c_l$ , extrapolated well beyond the normal stall angle. The extrapolated, linear lift curve is labeled "extended  $c_l$ " in the figure. In contrast, the Selig model (Ref. 13) is a weighted interpolation between the extended  $c_l$  and the airfoil table  $c_l$ , with a similar correction for  $c_d$ . In CAMRAD II, both stall-delay corrections are washed out angles of attack greater than 30 deg.

For Corrigan stall delay,

$$c_l = K_L c_{l\text{table}} \left( \frac{\alpha - \alpha_z}{K_L} + \alpha_z \right)$$

or

$$c_l = c_{l\text{table}} (\alpha - \alpha_z) + K_L c_{l\text{table}} \alpha_z$$

For Selig stall delay,

$$c_l = c_{ltable} + K_{sdL}(c_{lL} - c_{ltable})$$

$$c_d = c_{dtable} + K_{sdD}(c_{dL} - c_{dtable})$$

where

$$c_{lL} = c_{l\alpha}(\alpha - \alpha_z)$$

$$c_{dL} = c_{dz}$$

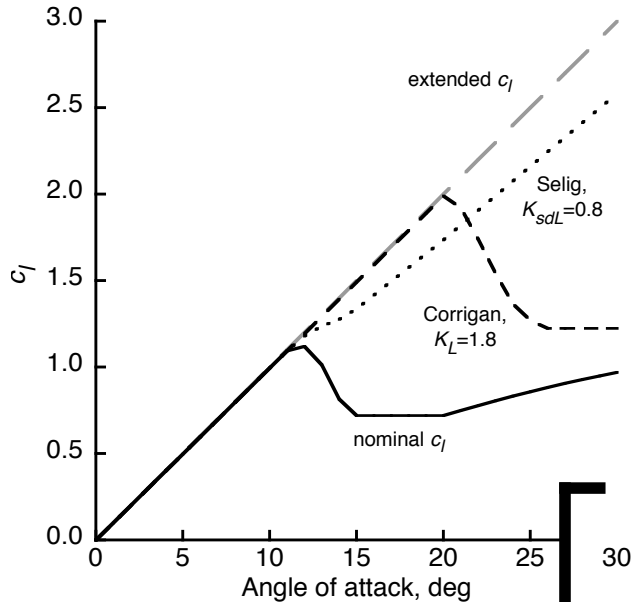


Fig. 4. 3-D stall delay models for the NACA 0012 airfoil.

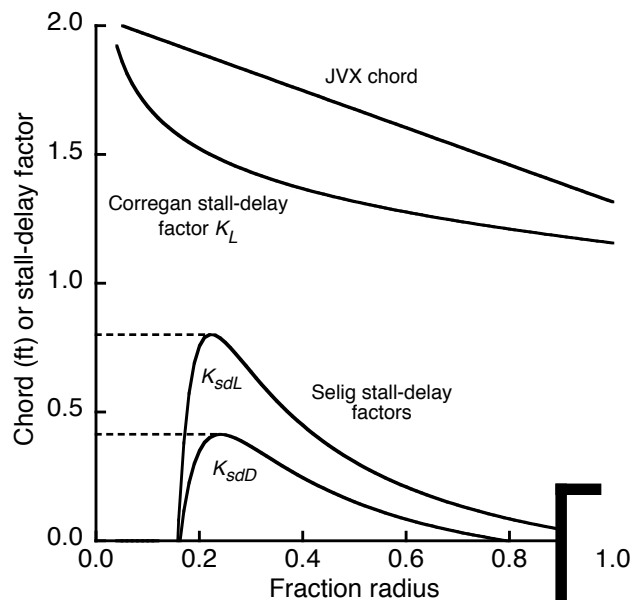


Fig. 5. 3-D stall delay factors vs. radius for the JVX planform.

Figure 5 shows the variations of stall-delay factors with radius for the JVX rotor (OARF configuration); the rotor chord is also plotted for reference. The Selig corrections are applied to lift and drag, with factors  $K_{sdL}$  and  $K_{sdD}$  respectively; the Corrigan model applies only to lift ( $K_L$ ). The Selig model is non-monotonic with radius, so for the CAMRAD II JVX model, the Selig stall-delay factors are set to their maximum values at extreme inboard radii (the dashed lines in the figure). For convenience, the default stall-delay model for JVX is the Selig model, but the choice of model makes negligible difference for JVX performance predictions.

### Hover Predictions

Most predictions of JVX hover performance reported here were made with a free-wake model, in which the shed vorticity is eventually rolled up into a single tip vortex (the rolled-up model). Predictions were also made with a multiple-trailer model, having a additional vortex trailer inboard of the radius at which blade-vortex interaction is experienced in hover. Three simpler models were also evaluated: uniform inflow, differential momentum, and prescribed wake. The effects of stall delay and Reynolds number corrections were also evaluated.

### Rolled-up free wake model

The CAMRAD II predictions of figure of merit  $FM$  are shown in Fig. 6 for the rolled-up wake model, with and without stall-delay corrections. This is the default CAMRAD II free-wake model, with a strong vortex at the tip, a weak vortex at the root, and a vortex sheet in between. It gives good correlation with the OARF test data at high  $C_T$ , but underpredicts figure of merit at low  $C_T$ . The multiple-trailer model used here is a simplified version of the one developed for TRAM in airplane mode (Ref. 10). It is discussed in more detail in the next subsection. It fits the JVX data better than the rolled-up model, especially at low to moderate thrust. However, it requires much more computer run time than the rolled-up model, so the latter, simpler wake model was used whenever possible. An example is calculation of the effects of 3-D stall delay, which are seen primarily at high thrust, where the rolled-up model is adequate. Results given in this paper are for the rolled-up wake model except where explicitly noted.

Predictions made with the rolled-up model, but without stall-delay corrections, are also shown in Fig. 6. Figure of merit is clearly underpredicted everywhere but very low thrust.

The Selig and Corrigan stall delay models are difficult to distinguish at the scale of Fig. 6, the difference being only about one line thickness at most. The effect of the CAMRAD II Reynolds number correction is of similar magnitude. Here, a 1/5-power-law correction is used. To better illustrate the differences,  $C_{P0}/\sigma$  is plotted in Fig. 7 for the two stall-delay models (with full Reynolds corrections). To reveal the effects of Reynolds number, predictions without the Reynolds corrections, but using the Selig stall-delay model, are also plotted. The difference between the two stall-delay models is clearly less than the effect of either alone compared to no stall delay, and the effect of Reynolds number is also small compared to the effect of stall delay. (The plot of  $C_{P0}/\sigma$  vs. thrust is almost identical for the rolled-up and multiple-trailer wake models, therefore the latter is not shown in Fig. 7.)

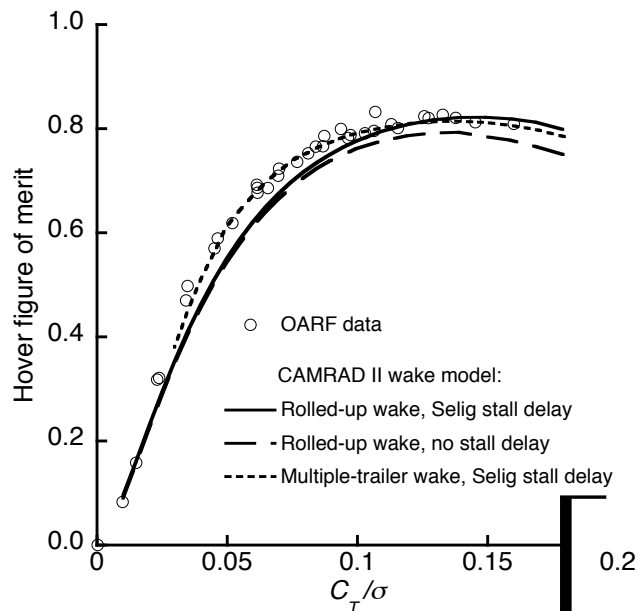


Fig. 6. CAMRAD II predictions of JVX hover figure of merit compared with OARF test data.

Figure 8 shows the effect of the stall-delay model on calculation of induced power, here plotted as the ratio  $\kappa$  of actual to ideal (momentum theory) induced power. The Selig and Corrigan predictions are nearly the same, so only the first is shown in Fig. 8. Stall delay reduces the induced power only at high thrust.

It is not surprising that predictions made with the Selig and Corrigan stall-delay models differ only slightly, given that both models were empirically adjusted to match experimental data. The small effect of Reynolds number is also to be expected, given the small difference in scale between the JVX rotor chord and the airfoils tested to develop the airfoil tables (Ref. 6).

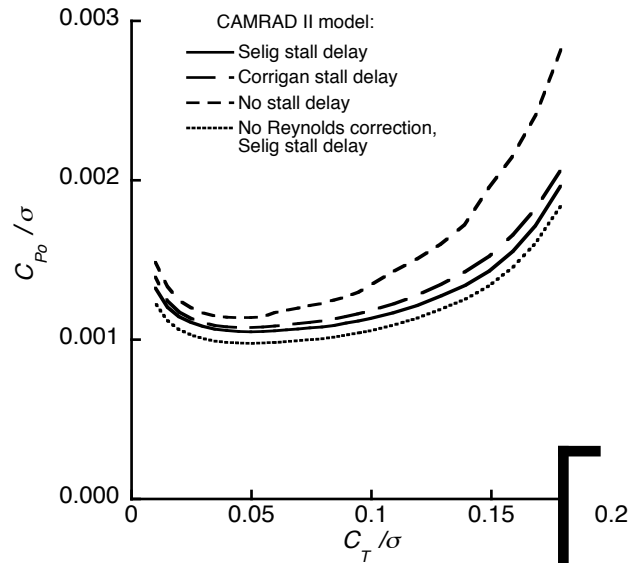


Fig. 7. CAMRAD II hover predictions of JVX  $C_{P0}/\sigma$  for different stall-delay models and Reynolds number corrections.

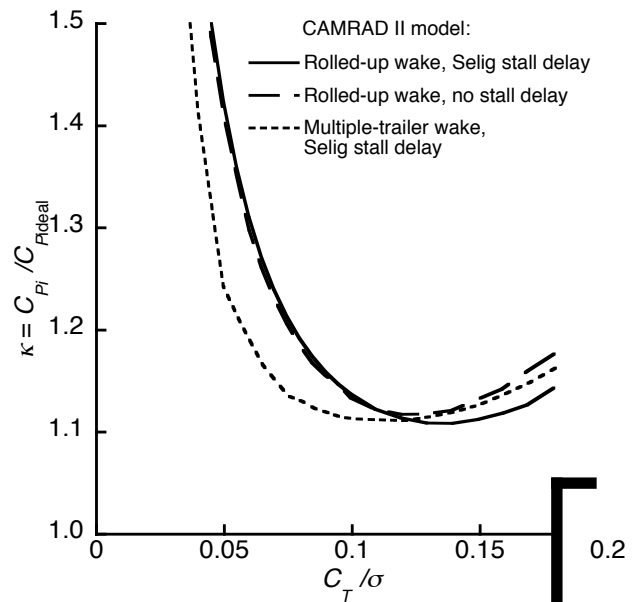


Fig. 8. CAMRAD II JVX hover predictions of  $\kappa$  with and without stall delay, and for the multiple-trailer wake model.

Figure 9 compares the rolled-up and multiple-trailer wake models with the TRAM 1/4-scale test data. The Selig stall-delay model was used for both sets of predictions. The improvement in predictions at low thrust can again be seen for the multiple-trailer model. The fit is not as good as for the JVX rotor (Fig. 6), probably because of the simplicity of the Reynolds number corrections (Ref. 10).

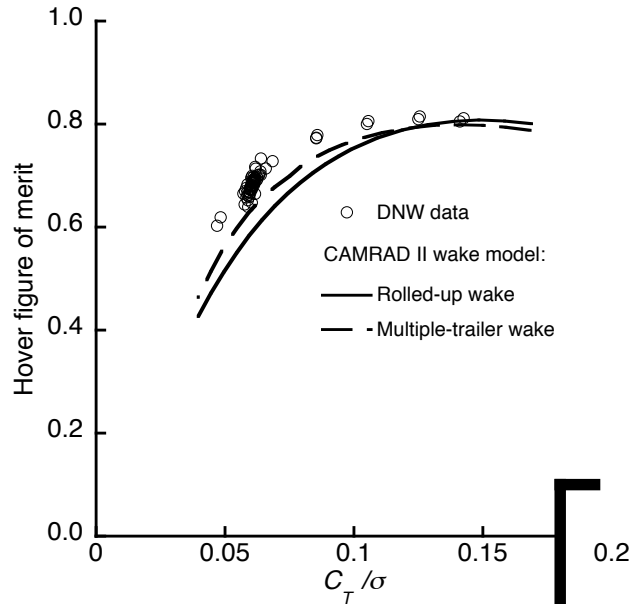


Fig. 9. CAMRAD II TRAM predictions of hover figure of merit compared with DNW test data.

### Multiple-trailer model

Some insight into the need for a multiple-trailer wake can be gained from a plot of circulation versus radius for different thrust levels (Fig. 10), here calculated with the rolled-up wake model. At low thrust, blade-vortex interaction can be seen slightly outboard of 90% radius. This is consistent with the results reported for TRAM in Ref. 9.

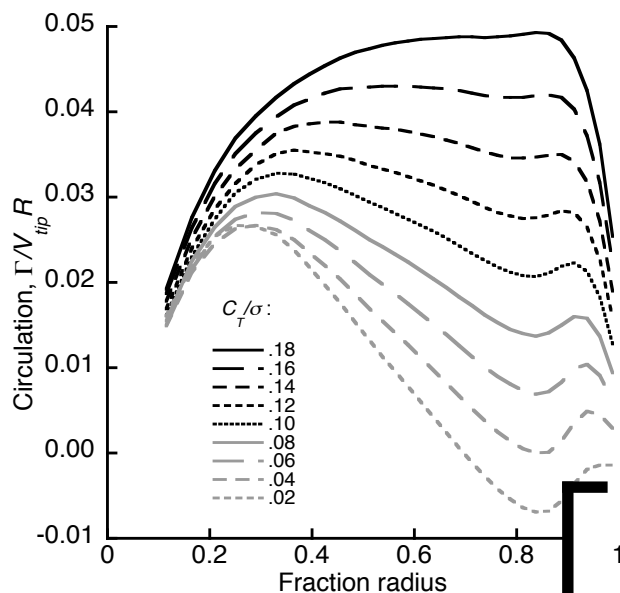


Fig. 10. JVX circulation vs. radius for different trimmed hover  $C_T/\sigma$ .

At high thrust, the rapid decrease in circulation near the tip results in a strong tip vortex. In the CAMRAD II rolled-up model, the strength of the tip vortex is determined from the peak bound circulation. Over the working portion of the blade (about 25-90% radius), circulation varies much more slowly, and the trailed vorticity is modeled with a vortex sheet, which is rolled up into the tip vortex (hence the name). At low thrust, however, this model breaks down: circulation decreases rapidly enough from 30% to 80% radius that the tip-vortex roll-up model is inadequate. Furthermore, at extremely low thrust, the angle of attack near the tip is negative, as is the circulation, hence the sign of the tip vortex. For highly twisted blades at low thrust, a conventional tip-vortex model is, therefore, invalid.

This problem is here addressed by adding a vortex trailer at 80% radius. CAMRAD II automatically assigns the appropriate sign and strength to each trailer (80%  $R$  and tip), derived from the circulation inboard of each trailer. In this model, the two trailers are independent and never combine into a single tip vortex. The improvement is significant (Fig. 6), but at considerable cost in computational time (up to an order of magnitude greater). Moreover, convergence is poor at low thrust. Convergence problems and computational time are closely related: methods of improving convergence include lower trim loop relaxation factors, additional wake iterations and sub-iterations, tighter tolerances on loop convergence, etc., all of which increase computational time. This reflects a fundamental difficulty: the physical wake is chaotic, so the more accurately it is modeled, the more inefficient the solution procedure becomes.

The most important addition to the multiple-trailer model to improve convergence was to specify slow core growth of the inboard vortex. The core grew from 0.2 mean chord at the blade to 1.0 chord after five rotor revolutions, with a square-law growth rate. All predictions shown here for the multiple-trailer wake used this core-growth model. Core growth was not required for convergence of the rolled-up model, so it was not there used.

The effect of the multiple-trailer wake on induced power is shown in Fig. 8. The shift in the induced-power curve relative to the rolled-up model mirrors the shift in figure of merit (Fig. 6).

It should be noted that the multiple-trailer model used here is distinct from the CAMRAD II “dual-peak” wake model. The latter is intended for use with negative tip loading, whereas the former applies to both positive and negative tip loading.

Because the purpose of this investigation is to develop methods of analysis for design optimization, an efficient model is imperative. Rotors are optimized for high thrust in hover, not low thrust, so the CAMRAD II rolled-up wake model is adequate in most cases. To date, the multiple-trailer model has not been developed further for the JVX rotor, but it has obvious potential.

A much more elaborate multiple-trailer model is also available in CAMRAD II, with up to one trailer per aerodynamic panel and an option to consolidate the trailers in the far wake (Ref. 10). That model, however, was developed for loads predictions in edgewise flight and has not been validated against hover data. Moreover, its computational requirements are exorbitant, at least for design optimization. Research on more complex models continues, but the rolled-up wake model is currently preferred for design optimization, and the model with one additional trailer is sufficient where increased accuracy is needed.

#### Additional hover models

Three additional, simpler aerodynamic models were also investigated. In increasing order of sophistication, they were uniform inflow, differential momentum theory (the CAMRAD II implementation of combined blade-element/momentum theory), and a prescribed wake model, here the Kocurek and Tangler model (Ref. 14). Figure 11 suggests that they all match the test data better than the rolled-up free wake model, but this is misleading. All three models rely upon empirical adjustments for good predictions of figure of merit. Figure 12 shows  $C_{P0}/\sigma$  for each model, which better reveals their differences (compare Fig. 7).

Figure 13 shows predictions of the ratio  $\kappa$  of actual to ideal induced power for the three simpler models. The curve for uniform inflow would be flat if not for numerical effects at very low thrust. The differential-momentum predictions generally match the pattern of the free-wake models (Fig. 8), but the prescribed-wake model varies considerably.

The uniform inflow and differential momentum models rely on an empirical factor on induced velocity,  $\kappa_\lambda$ , for a good fit to the data. To match the JVX hover data,  $\kappa_\lambda=1.10$  for uniform inflow, and  $\kappa_\lambda=1.04$  for differential momentum. Although these two models may give good fits to the data with appropriate values of  $\kappa_\lambda$ , they cannot be relied upon to give good performance estimates as blade design parameters are varied, because there is no way to determine in advance the correct values of  $\kappa_\lambda$ .

Worse, these two models cannot possibly account for the effects of wake distortion and vortex interactions. (However, they may be acceptable for high-speed axial flow, where the wake is less important.)

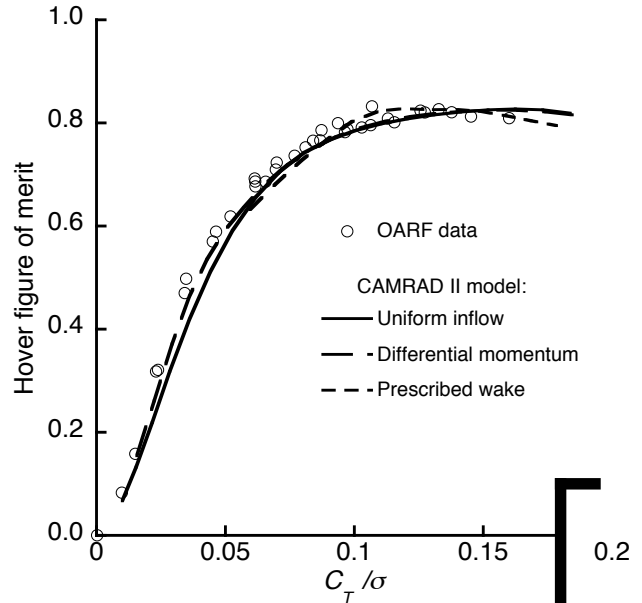


Fig. 11. CAMRAD II hover predictions of JVX figure of merit for three simplified aerodynamic models.

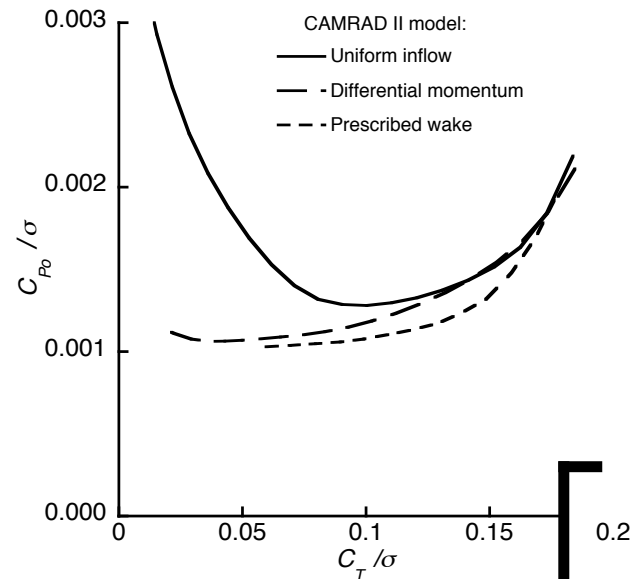


Fig. 12. CAMRAD II hover predictions of JVX  $C_{P0}/\sigma$  for three simplified aerodynamic models.

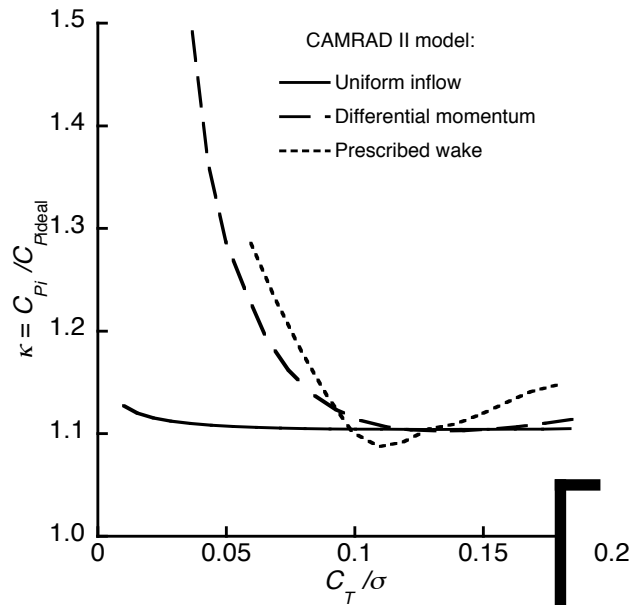


Fig. 13. CAMRAD II JVX hover predictions of  $\kappa$  for three simplified aerodynamic models.

The Kocurek and Tangler prescribed wake model would seem to be a candidate for performance analysis, but it too depends upon empirical adjustments, notably a factor on vertical convection. Moreover, the Kocurek and Tangler model estimates the vertical convection as a function of blade twist, number of blades, and  $C_T$  (complete equations are given in Refs. 4 and 14). This model is mathematically invalid for large twist rates at low  $C_T$ , which occurs below about  $C_T/\sigma=0.05$  for the JVX rotor.

More advanced prescribed wake models are certainly possible, and the Kocurek and Tangler model itself could conceivably be modified to work better with the JVX rotor. The CAMRAD II free-wake model is not completely free of empiricism; for example, the initial radial position of the tip vortex must be specified. Nevertheless, this model is not as dependent on the details of the blade design, in particular twist, as is the Kocurek and Tangler model. The free-wake model by design self-adjusts the wake geometry to match the particulars of the rotor design and operating condition, and does not rely upon empirical adjustments to induced velocity. Furthermore, CAMRAD II gains very little savings in computer time with a prescribed wake model, compared to the rolled-up free wake model. For these reasons, prescribed wake models were not pursued further in the present study. However, an efficient prescribed wake model may prove useful for initialization of the free wake geometry, so an opportunity exists for further development of prescribed wake models.

## Airplane-Mode Predictions

The JVX airplane-mode data are plotted as propulsive efficiency  $\eta$  versus thrust in Fig. 14. (Predictions are not shown, so as not to obscure the data.) The data fall into a well-ordered pattern, but no single advance ratio  $\mu$  has data that span the full range of thrust. The data are re-plotted as power versus thrust in Fig. 15. Here, the clustering into five groups of constant  $\mu$  is obvious, as is the good fit of CAMRAD II predictions to the data. All data at  $\mu=0.523$  and below were taken at 487 rpm, but the data at  $\mu=0.562$  were taken at 531 rpm. The CAMRAD II predictions were made with the rolled-up free wake model. 3-D stall delay is not relevant at high speed, so no stall delay model was used.

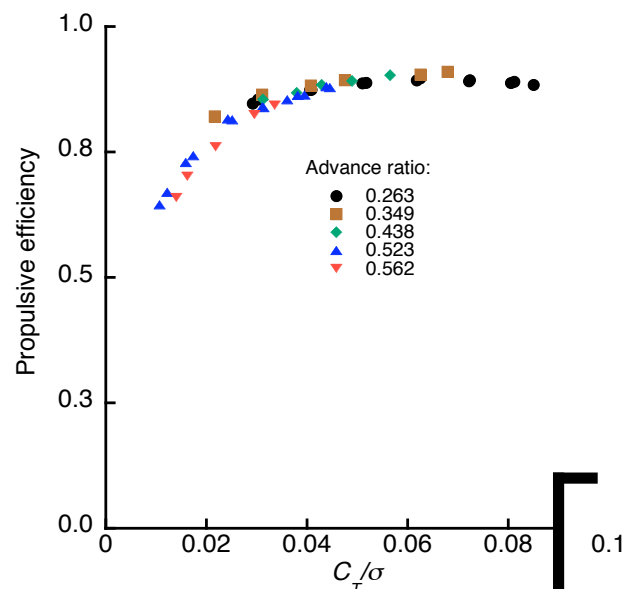


Fig. 14. Measured JVX rotor propulsive efficiency from the NFAC Phase II test.

Airplane-mode performance predictions were made with three other CAMRAD II aerodynamic models: uniform inflow, differential momentum, and the Kocurek and Tangler prescribed-wake model (the same models used for hover predictions). All three were empirically adjusted for the best fit to the data in the same manner as for the hover predictions. The differences in both  $\eta$  and  $C_P/\sigma$  are extremely small, usually less than one line thickness at the scale of Figs. 14 and 15. The calculations with the greatest differences are shown in Figs. 16 and 17 for the two advance ratios with the most data points ( $\mu=.263$  and  $\mu=.523$ ). The Kocurek and Tangler model differs slightly from the free-wake model at  $\mu=.263$ , and the uniform-inflow model differs noticeably at  $\mu=.523$ , most evidently in Fig. 17. However, the discrepancy in the uniform-inflow model is greatest at combined high thrust and high  $\mu$ , where no test data exist for comparison. Predictions

made with differential momentum theory are always extremely close to the free-wake predictions, and are therefore not shown.

The multiple-trailer model was not used here, because blade-vortex interaction does not exist at high-speed axial flow, even at low thrust. Moreover, differential momentum theory gives as good a fit to the data as the free-wake and prescribed-wake models. There is, therefore, no advantage to be gained from higher-order wake models.

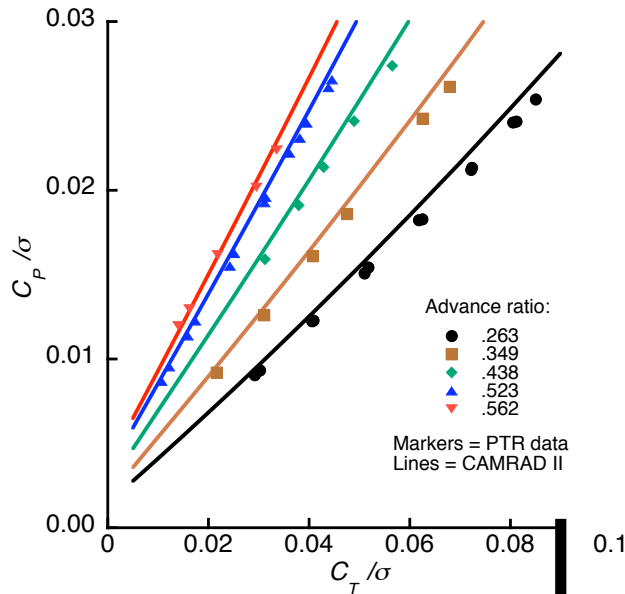


Fig. 15. CAMRAD II predictions of JVX airplane-mode power  $C_p/\sigma$  compared with test data.

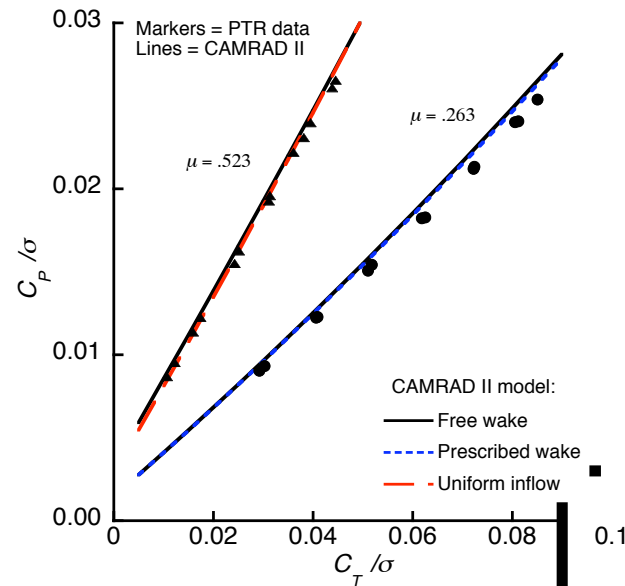


Fig. 16. Predictions of  $C_p/\sigma$  made with three different aerodynamic models compared with JVX test data.

Although the CAMRAD II free-wake and differential-momentum models fit the data quite well, there remains a slight overprediction of power, especially at low  $\mu$ . The mismatch is not seen in predictions made for the TRAM model; at least, the mismatch is much smaller (Figs. 18 and 19). The scales of Figs. 18 and 19 have been expanded for better legibility, which exaggerates the mismatch compared to Figs. 15-17. However, the TRAM data extend over smaller ranges of thrust and  $\mu$  than do the JVX data, so the comparison is not definitive. (The TRAM data presented here are the same as in Ref. 10.)

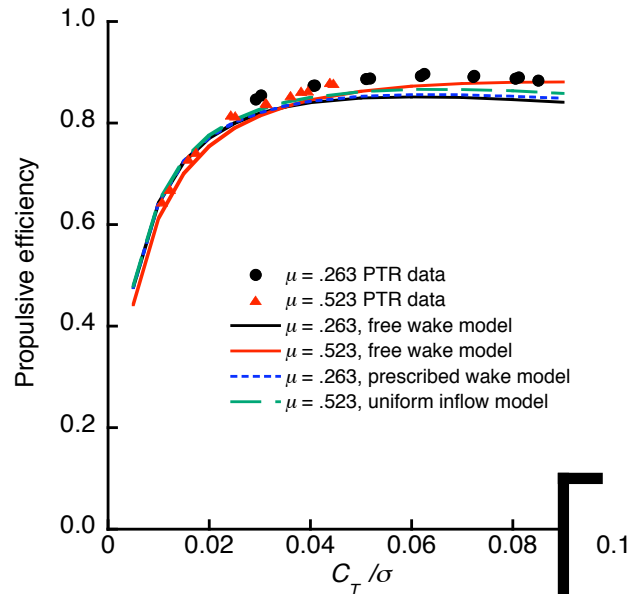


Fig. 17. Predictions of JVX propulsive efficiency made with three different aerodynamic models compared with test data.

Possible reasons for the mismatch between CAMRAD II predictions and JVX airplane-mode data may be summarized in four categories: blade modeling errors, limitations in the CAMRAD II wake model, airfoil table deficiencies, and test data errors. The good fit to JVX hover data makes the first two possibilities unlikely, as does the good fit to TRAM airplane-mode data. The limited range of TRAM airplane-mode data leaves open a slight possibility of problems with the airfoil tables at high Mach numbers. Finally, known limitations of the JVX airplane-mode test data, discussed briefly below, make this a likely source of the problem, but this hypothesis has not been proved.

Reference 3 mentions concerns about JVX Phase I spinner tare corrections. Good spinner tare data are available only for the Phase I test, but the Phase II data are more consistent than the Phase I data. The improved consistency and more comprehensive test conditions were motivations for examining only the Phase II data in detail.

Attempts to directly measure spinner force during Phase II gave unrealistic results. Because it is possible that the Phase II test data still contain residual tare errors, no significant effort was expended to improve the match between CAMRAD II performance predictions and JVX test data (Figs. 15-17). With the rotor destroyed, there is no way to confirm the spinner tares or any similar hypothesis for the mismatch between predictions and data. (A discussion of TRAM tare corrections is given in Ref. 10.)

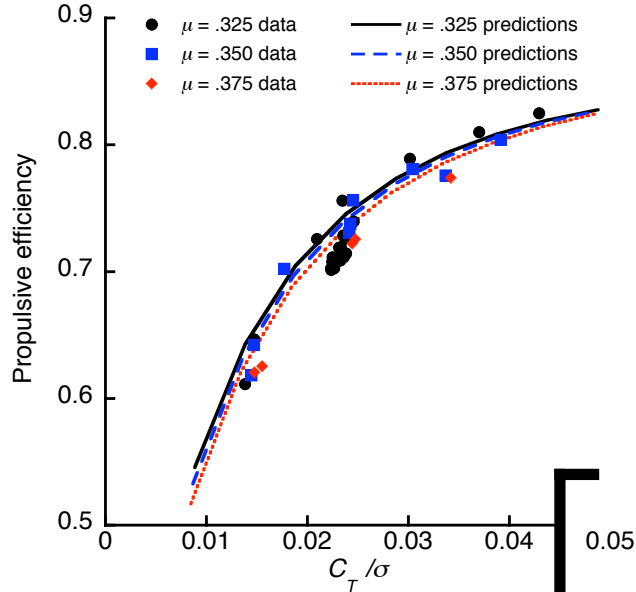


Fig. 18. TRAM isolated rotor measured and predicted propulsive efficiency.

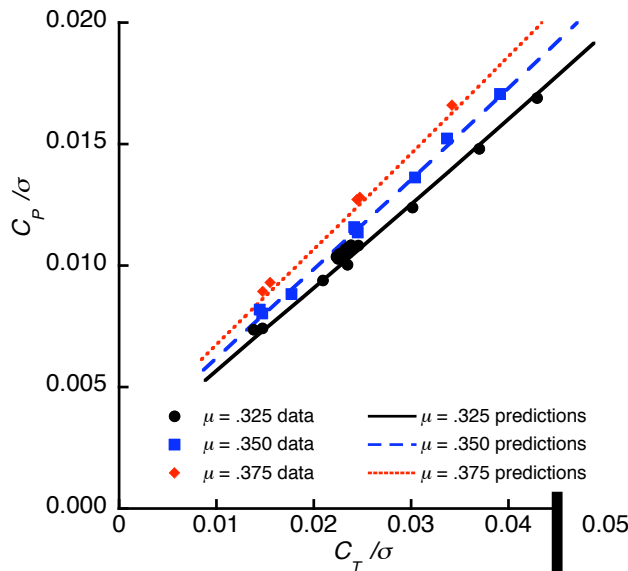


Fig. 19. TRAM isolated rotor measured and predicted power (airplane mode).

## Conclusions

Predictions of JVX rotor performance were compared with two sets of test data, for hover and airplane mode (high-speed axial flow). Several different CAMRAD II aerodynamic models were used to determine the appropriate level of sophistication for rotor design optimization. The effects of Reynolds number corrections and two different stall-delay models were examined.

A free-wake model with a single tip vortex matched the hover data well at high thrust, but a multiple-trailer model was needed for accuracy at low thrust. However, the multiple-trailer model was much less efficient than the conventional model, in which the shed vorticity was rolled up into the single tip vortex. Prescribed-wake (Kocurek and Tangler), differential-momentum and uniform-inflow models could all be empirically adjusted for a good fit to hover performance data, but had limitations rendering them unsuitable for design optimization, at least for hover.

Either of two stall-delay models proved adequate for hover. Reynolds number corrections made only a small difference at this scale, as was to be expected given the small difference in scale between the JVX rotor chord and the airfoils tested to develop the airfoil tables.

Equally good fits to airplane-mode data were achieved for differential-momentum, prescribed-wake, and free-wake models; a slightly worse, but still reasonable, fit was achieved with uniform inflow. Spinner tare issues were a possible source of a residual mismatch to airplane-mode data, most noticeable at lower advance ratios.

For proprotor design studies, the conventional rolled-up free-wake model is recommended for hover predictions as the best compromise between accuracy and efficiency. A differential-momentum model is recommended for airplane mode because of its good accuracy and high efficiency. Occasional cross checks with the multiple-trailer model in hover and the rolled-up free-wake model in airplane mode may be in order to verify the accuracy of design optimizations.

## Acknowledgements

The author wishes to express his appreciation to Randy Peterson for recovering the JVX Phase II airplane-mode data, and to Wayne Johnson for his patient assistance in planning and conducting the research.

## References

1. Johnson, W., Yamauchi, G. K., and Watts, M. E., "NASA Heavy Lift Rotorcraft Systems Investigation," NASA TP-2005-213467, September 2005.
2. Felker, F. F., Signor, D. B., Young, L. A., and Betzina, M. D., "Performance and Loads Data From a Hover Test of a 0.658-Scale V-22 Rotor and Wing," NASA TM-89419, April 1987.
3. Felker, F. F., "Results from a Test of a 2/3-Scale V-22 Rotor and Wing in the 40- by 80-Foot Wind Tunnel," AHS 47th Annual Forum, Phoenix, Arizona, May 1991.
4. Johnson, W., "CAMRAD II Comprehensive Analytical Model of Rotorcraft Aerodynamics and Dynamics," Johnson Aeronautics, Palo Alto, California, 2007.
5. Johnson, W., "Influence of Wake Models on Calculated Tiltrotor Aerodynamics," AHS Aerodynamics, Acoustics, and Test and Evaluation Technical Specialists Meeting, San Francisco, California, January 2002.
6. Jenks, M. D.; and Narramore, J. C.: Final Report for the 2-D Test of Model 901 Rotor and Wing Airfoils (BSWT 592). Bell-Boeing Report No. D901-99065-1, May 1984.
7. Narramore, J. C., Platz, D. A., and Brand, A. G., "Application of Computational Fluid Dynamics to the Design of the BA 609," 25th European Rotorcraft Forum, Rome, Italy, September 1999.
8. Young, L. A., Booth, E. R., Yamauchi, G. K., Botha, G., Dawson, S., "Overview of the Testing of a Small-Scale Proprotor," American Helicopter Society 55th Annual Forum, Montréal, Canada, May 1999.
9. Potsdam, M. A., and Strawn, R. C., "CFD Simulations of Tiltrotor Configurations in Hover," American Helicopter Society 58th Annual Forum, Montréal, Canada, June 2002.
10. Johnson, W., "Calculation of Tilt Rotor Aeroacoustic Model (TRAM DNW) Performance, Airloads, and Structural Loads," AHS Aeromechanics Specialists' Meeting, Atlanta, Georgia, November 2000.
11. McCluer, M., "Tiltrotor Hover Performance Comparisons," Presented at the Naval Air Systems Command Air Vehicle Engineering Conference, La Jolla, California, May 21-23, 2002.
12. Corrigan, J. J., and Schillings, J.J., "Empirical Model for Stall Delay Due to Rotation," AHS Aeromechanics Specialists Conference, San Francisco, California, January 1994.
13. Du, Z., and Selig, M.S., "A 3-D Stall-Delay Model for Horizontal Axis Wind Turbine Performance Prediction," AIAA Paper 98-0021, January 1998.
14. Kocurek, J. D., and Tangler, J. L., "A Prescribed Wake Lifting Surface Hover Performance Analysis," American Helicopter Society 32nd Annual Forum, Washington, D.C., May 1976.